Sedimentology (2002) **49,** 483–503

Geometry and grain-size sorting of ripples on low-energy sandy beaches: field observations and model predictions

JEFFREY S. DOUCETTE
Department of Geography, University of Western Australia, 35 Stirling Highway, Crawley, WA 6009, Australia (E-mail: jdoucett@geog.uwa.edu.au)

ABSTRACT

There are very few field measurements of nearshore bedforms and grain-size distribution on low-energy microtidal beaches that experience low-amplitude, long-period waves. Field observations are needed to determine grain-size distribution over nearshore bedforms, which may be important for understanding the mechanisms responsible for ripple development and migration. Additional nearshore field observations of ripple geometry are needed to test predictive models of ripple geometry. Ripple height, length and sediment composition were measured in the nearshore of several low-energy beaches with concurrent measurements of incident waves. The distribution of sediment sizes over individual ripples was investigated, and the performance of several models of ripple geometry prediction was tested both spatially and temporally. Sediment samples were collected from the crest and trough of 164 ripples. The sand-sized sediment was separated from the small amount (generally <3%) of coarser material (>2 mm) that was present. Within the sand-sized fraction, the ripple crests were found to be significantly coarser, better sorted and more positively skewed than the troughs. Overall, the troughs were finer than the crests but contained a greater proportion of the small fraction of sediment larger than 2 mm. The field model of Nielsen (1981) and the model of Wiberg & Harris (1994) were found to be the most accurate models for predicting the wavelength of parallel ripples in the nearshore of the low-energy microtidal environments surveyed. The Wiberg & Harris (1994) model was also the most accurate model for predicting ripple height. Temporal changes in ripple wavelength appear to be dependent on the morphological history of the bed.

Keywords Bedforms, grain size, low-energy beaches, ripple geometry.

INTRODUCTION

Ripple geometry and grain-size distribution over bedforms are poorly understood in the field. Although there have been several studies of nearshore grain size on the cross-shore distribution of sand sizes (e.g. Inman, 1953; Miller & Zeigler, 1958; Greenwood & Davidson-Arnott, 1972; Medina *et al.*, 1994), longshore patterns (e.g. McLaren & Bowles, 1985; Masselink, 1992; Sanderson & Eliot, 1999) and the use of grain-size distributions to determine sediment transport pathways (e.g. Kench, 1998), there have been no field examinations of the small-scale grain-size distribution over individual ripples in the nearshore of low-energy beaches with low-amplitude, long-period waves. Although several laboratory studies have addressed this issue (Noda, 1968; De Best & Bijker, 1971; Carter *et al.*, 1973; Foti, 1993; Foti & Blondeaux, 1995), Inman (1957) provided the only field study that has looked comprehensively at grain-size differences between the crests and troughs of ripples, although Inman (1957) collected few samples from the nearshore region. A knowledge of sediment size distribution over nearshore bedforms may aid in understanding the mechanisms involved in ripple formation, ripple constraints on sediment suspension and ripple migration.

It is important to be able to predict the geometry of nearshore bedforms because they induce frictional drag effects, which must be estimated before calculations of sediment transport by waves and currents can be made (Grant & Madsen, 1982; Li, 1994; Li *et al.*, 1996; Mathisen & Madsen, 1996). Additionally, although numerous models exist for predicting ripple geometry, they have been found to perform poorly in nearshore environments (Vincent & Osborne, 1993; Osborne & Vincent, 1993; Dick *et al.*, 1994; Vincent *et al.*, 1999). There is a general lack of ripple geometry measurements in the nearshore region and, more specifically, no ripple geometry measurements exist from nearshore low-energy beaches where long-period, low-amplitude waves occur. Current predictive models for ripple geometry perform well under the conditions for which they were designed, which mainly involve uniform wave and sediment characteristics, because they were mostly derived from laboratory observations. However, the usefulness of these models for application to low-energy nearshore environments with low-amplitude, long-period waves and more poorly sorted sediment is unknown. The significance of any differences in sediment distribution over the bedforms to the resulting ripple geometry is also not fully understood.

This study aims to (i) determine the difference in grain-size distribution between ripple crests and troughs; (ii) test the sensitivity of ripple prediction models to input of mean crest and trough grain sizes; and (iii) evaluate some popular models for predicting ripple geometry for use in the nearshore zone of low-wave energy beaches. The central coast of Western Australia provided an ideal environment to accomplish these aims because of the relatively calm, clear water and the presence of long-crested parallel ripples immediately seaward of the beach face at many easily accessible, low-energy beaches. Here, the term low energy refers to modal significant wave heights of <1·0 m and commonly <0·5 m over at least 12 months of observation.

FIELD SITES

The field sites were located on the central west coast of Western Australia between Coolimba and Garden Island (Fig. 1). All field sites were low-energy, microtidal, non-cohesive sandy beaches and were sampled between 10 December 1999

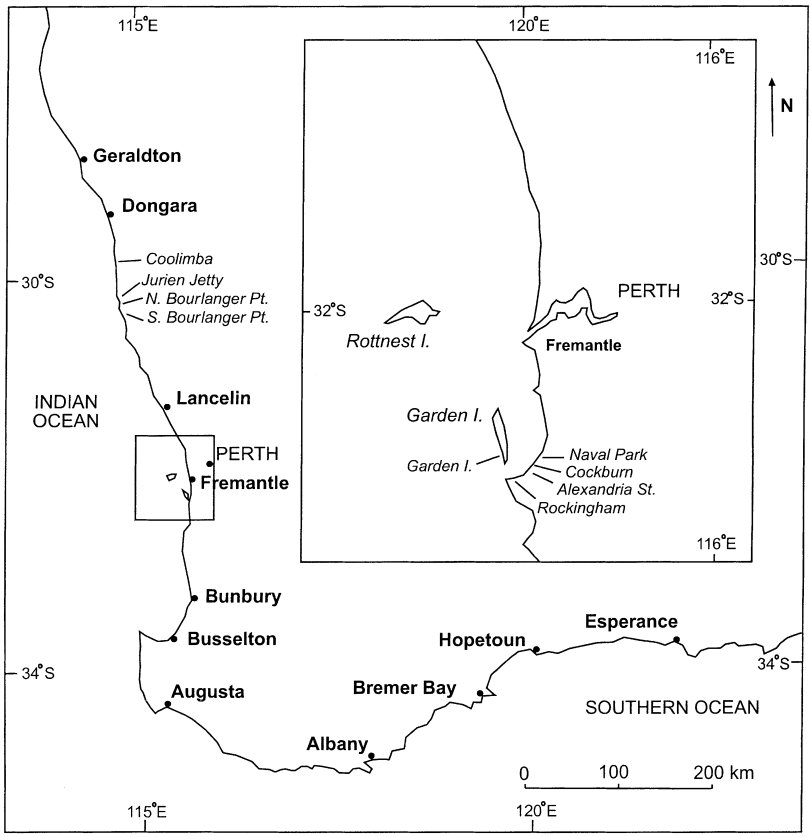

Fig. 1. Location of field sites.

and 5 January 2000 except for the temporal measurements at Garden Island, which were made from 17 to 19 February 1999. Tides are predominantly diurnal with a spring tidal range (MLLW to MHHW) of 0·4 m and a lowest to highest astronomical tidal range (LAT to HAT) of 1·1 m (Department of Defence, 2000). The beaches experience low-energy wave conditions, where average annual significant wave height is <1 m as a result of shelter provided by islands (e.g. Naval Park), offshore reef (e.g. Garden Island) or both (e.g. Jurien Jetty). The field sites were selected for their range in mean grain sizes (D = 0·3–0·85 mm) and the presence of distinct parallel ripples in the nearshore region. Low-energy conditions allowed clear underwater views of the bedforms for ease and accuracy of sediment sampling and geometry measurements. Significant wave heights among the field sites were between 0·06 m and 0·26 m, and significant wave periods ranged from 2·2 s to 12·2 s. Ripple wavelengths (λ) were 0·08 m to 0·95 m and heights (η) were 0·02 m to 0·16 m. The sediment was composed of mixed calcareous and quartzose sands.

EXPERIMENTAL DESIGN

Spatial observations

Waves and ripple dimensions were measured and sediment samples were collected across the nearshore of nine low-energy beaches in central and south-western Western Australia (Fig. 1). Waves were measured with a Druck pressure sensor at 4 Hz for 17 min, or 4096 data points, at one to five locations cross-shore at each site. The dimensions of a total of 164 subaqueous ripples were measured, and sediment samples were taken from the crests and troughs of each ripple. Samples of 20–90 g were taken from the upper 0·01–0·02 m of sediment to avoid possible effects of armouring in the trough. Ripple wavelengths were measured adjacent to where the samples were taken by placing a clear Plexiglass strip across the crests. Positions of each ripple crest were marked with a grease crayon on the Plexiglass (Inman, 1957). Ripple heights were measured by sliding the Plexiglass sheet through the ripple crest and marking it at the sand surface. Errors in ripple wavelength measurement were up to ±1 cm, whereas height measurements were accurate to within ±0·5 cm. Cross-shore profiles were surveyed using a standard level and stadia rod.

Temporal observations

Measurements of ripple wavelengths, currents and waves were made for 46 h on a low-energy beach at Garden Island (Fig. 1). Ripple wavelengths were measured every half hour, and waves and currents were measured at 4 Hz. Large ripples (wavelength, $\lambda = 0{\cdot}3$–$1{\cdot}2$ m; height, $\eta = 0{\cdot}05$–$0{\cdot}15$ m) with crests parallel to the shore were present in coarse sand (D = 0·66–0·74 mm). Ripple crest positions were recorded along two survey lines established perpendicular to shore from mid-swash to ≈10 m offshore. A measuring tape was secured to the bed along each line, and the positions of the ripple crests were recorded every 30 min. Waves were recorded by a Druck pressure sensor, and currents were recorded by a Marsh McBirney 512 electromagnetic current meter mounted at 0·20 m above the bed. Both instruments sampled at 4 Hz, and the current meter sampling volume was a sphere with a radius of 3·8 cm.

SEDIMENT SIZE ANALYSIS

All 328 sediment samples were analysed using a settling tube, which was 2 m tall and 0·14 m in diameter. The settling tube was used instead of sieve analysis for several reasons. First, it is much quicker than sieve analysis, and the large number of samples required a relatively easy and quick technique. Secondly, only small amounts of sand could be obtained from some of the smaller ripples, which were not large enough for sieve analysis. Thirdly, generally 98% of the sediment was in the sand size range (0·0625–2 mm), which is the ideal size for settling tube analysis. Fourthly, as the settling tube determines the size distribution based on the fall velocities of the sediment, a better representation of the hydraulic properties of the irregular shaped carbonate sands was obtained (Kench & McLean, 1997). Lastly, settling tube analysis is used in many coastal bedform studies (e.g. Inman, 1957; Miller & Komar, 1980; Osborne & Greenwood, 1993; Black & Oldman, 1999), thus allowing direct comparisons.

Before the sediment was put through the settling tube, it was sieved through a 2-mm (−1 phi) sieve to recover the sand-sized fraction. The proportion of the total sample >2 mm was calculated, and most samples had between 0% and 3% material coarser than 2 mm. A few samples had up to 12% coarser material, with

one sample possessing 15%. After the larger sediment was removed, the samples were split mechanically to obtain small subsamples of 2–5 g for analysis in the settling tube. Each sample was run through the settling tube three times, and the results of all three runs were summed for each sample. This method provides a better representation of the size distribution of the whole sample, and any errors in settling tube operation could be detected by comparison of all three runs. The settling tube had a high precision, as the maximum coefficient of variation of the mean settling velocity was <6% (Hegge, 1994). The settling velocities were converted to equivalent grain sizes using the technique described by Hallermeier (1981).

MODELS FOR THE PREDICTION OF RIPPLE GEOMETRY

Several models for the prediction of ripple geometry, namely those of Nielsen (1981), Grant & Madsen (1982), Wikramanayake (1993), Mogridge *et al.* (1994) and Wiberg & Harris (1994), were used to compare measurements of ripple geometry in the field. Each model was run three times, once using grain-size input from the crest, once with grain-size input from the ripple trough and once with an average of the crest and trough grain sizes.

The models generally require input of a mean or median grain size, nearbed orbital diameter and wave period. The mean or median grain size was calculated from the settling tube output. The hydrodynamic parameters were calculated from 8192 data points or ≈17-min records. Nearbed orbital diameter (d_o) was calculated using linear theory as

$$d_o = \frac{H}{\sinh(kh)} \tag{1}$$

where H is significant wave height, h is mean depth and k is the wavenumber ($2\pi/L$).

Models of Nielsen (1981)

Nielsen (1981) developed two sets of equations for the prediction of ripple geometry: For field conditions:

$$\lambda/a_s = \exp[(693 - 0{\cdot}37\ln^7\psi)/(1000 + 0{\cdot}75\ln^8\psi)] \tag{2}$$

$$\eta/a_s = 21\psi^{-1{\cdot}85} \tag{3}$$

For laboratory conditions:

$$\lambda/a_s = 2{\cdot}2 - 0{\cdot}345\psi^{-0{\cdot}34} \tag{4}$$

$$\eta/a_s = 0{\cdot}275 - 0{\cdot}022\sqrt{\psi} \tag{5}$$

where ψ is the mobility number

$$\psi = \frac{(a_s\omega)^2}{(s-1)gD} \tag{6}$$

and where a_s is the nearbed wave orbital amplitude ($d_o/2$) calculated from linear theory, ω is the wave radian frequency ($2\pi/T$), s is the specific density of sand, g is the acceleration resulting from gravity and D is the mean grain diameter. The relationships predicted by Nielsen (1981) were derived from data from the laboratory studies of Yalin & Russell (1962), Kennedy & Falcon (1965), Mogridge & Kamphuis (1972), Carstens *et al.* (1969), Dingler (1974), Nielsen (1979) and field studies of Inman (1957), Dingler (1974) and Miller & Komar (1980). Laboratory conditions refer to monochromatic waves generally used in laboratory wave basins, whereas field conditions refer to a broader wave spectra as would be found under natural conditions.

Model of Grant & Madsen (1982)

Grant & Madsen (1982) predicted ripple geometry based on local skin friction and suggested two different relationships based on observations first made by Inman (1957) and on the wave tank data of Carstens *et al.* (1969). The first relationship is known as the equilibrium range, where ripple steepness (height to length ratio, η/λ) is near a maximum and the ripple wavelength scales with the nearbed wave orbital amplitude. The second relationship is known as the break-off range, where the ripple wavelength is no longer correlated with nearbed wave orbital amplitude and the ripple steepness decreases. The transition between the two ripple regimes is called the break-off point and is defined by the break-off Shields parameter, θ_B,

$$\theta_B = 1{\cdot}8\theta_{cr}S_*^{0{\cdot}6} \tag{7}$$

where θ_{cr} is the sediment threshold Shields parameter and S_* is a dimensionless sediment parameter

$$S_* = (D/4v)[(s-1)gD]^{0{\cdot}5} \tag{8}$$

where ν is the kinematic viscosity of water. The van Rijn (1989) definition of θ_{cr} was used here where

$$\theta_{cr} = 0{\cdot}24(D_*)^{-1} \quad \text{for } D_* \leq 4 \tag{9}$$

$$\theta_{cr} = 0{\cdot}14(D_*)^{-0{\cdot}64} \quad \text{for } 4 < D_* \leq 10 \tag{10}$$

$$\theta_{cr} = 0{\cdot}04(D_*)^{-0{\cdot}10} \quad \text{for } 10 < D_* \leq 20 \tag{11}$$

$$\theta_{cr} = 0{\cdot}013(D_*)^{0{\cdot}29} \quad \text{for } 20 < D_* \leq 150 \tag{12}$$

$$\theta_{cr} = 0{\cdot}055 \quad \text{for } D_* > 150 \text{ and} \tag{13}$$

$$D_* = d_{50}\left[(s-1)g/\nu^2\right]^{\frac{1}{3}} \tag{14}$$

The equilibrium range occurs when $\theta < \theta_B$ where θ is the maximum skin friction wave Shields parameter

$$\theta = \frac{u_{*_{wm}}^2}{(s-1)gD} \tag{15}$$

and $u_{*\mathrm{wm}}$ is the maximum skin friction wave shear velocity

$$u_{*_{wm}} = (f_w/2)^{0{\cdot}5} u_m \tag{16}$$

where $u_{*\mathrm{m}}$ is the mean nearbed orbital velocity. For simplicity and consistency, the wave friction factor f_{w} is estimated here using the definition of Swart (1974)

$$f_w = \exp\left[5{\cdot}213(k_s/a_s)^{0{\cdot}194} - 5{\cdot}977\right] \tag{17}$$

where k_s is the bed roughness height approximated as $2{\cdot}5D$ for smooth beds.

For ripples in the equilibrium range ($\theta < \theta_{\mathrm{B}}$)

$$\eta = 0{\cdot}22a_s(\theta/\theta_{cr})^{-0{\cdot}16} \tag{18}$$

$$\lambda = 6{\cdot}25\eta(\theta/\theta_{cr})^{0{\cdot}04} \tag{19}$$

For ripples in the break-off range ($\theta > \theta_{\mathrm{B}}$)

$$\eta = 0{\cdot}48a_s(\theta/\theta_{cr})^{-1{\cdot}5} \tag{20}$$

$$\lambda = 3{\cdot}6\eta S_*^{-0{\cdot}6}(\theta/\theta_{cr}) \tag{21}$$

Model of Wikramanayake (1993)

Wikramanayake (1993) related ripple wavelength to the non-dimensional parameter, Z, by

$$Z = \frac{\theta 4\nu}{\sqrt{(s-1)gd_{50}^3}} \tag{22}$$

where d_{50} is the median grain size, which is also used by Wikramanayake (1993) instead of mean grain-size diameter (D) when calculating θ.

For $0{\cdot}0016 < Z < 0{\cdot}012$

$$\lambda = 0{\cdot}120\frac{u_m}{\omega}Z^{-0{\cdot}49} \tag{23}$$

$$\eta = 0{\cdot}018\frac{u_m}{\omega}Z^{-0{\cdot}50} \tag{24}$$

and for $0{\cdot}012 < Z < 0{\cdot}18$

$$\lambda = 0{\cdot}0667\frac{u_m}{\omega}Z^{-0{\cdot}58} \tag{25}$$

$$\eta = 0{\cdot}0007\frac{u_m}{\omega}Z^{-1{\cdot}23} \tag{26}$$

When $Z > 0{\cdot}18$, it is assumed that sheet flow conditions apply and the bed is flat.

Model of Mogridge *et al.* (1994)

The Mogridge *et al.* (1994) model for predicting maximum ripple wavelength is dependent on the wave period parameter χ,

$$\chi = \frac{\rho D}{\gamma_s T^2} \tag{27}$$

where γ_s is the specific weight of sediment. The wave period parameter differs from the mobility number in its omission of the nearbed wave orbital amplitude. When $\chi < 0{\cdot}15 \times 10^{-6}$, the maximum ripple wavelength is predicted as a function of mean grain diameter where

$$\lambda = 1394D \tag{28}$$

and λ is independent of the wave period parameter. This relationship was derived from field data from a number of studies and is suggested for use in predicting ripple wavelengths in the field. At higher values of the wave period parameter ($\chi > 0{\cdot}15 \times 10^{-6}$), which mostly occur under laboratory conditions, the ripple wavelength is predicted by

$$\log_{10}(\lambda/D) = 13{\cdot}373 - 13{\cdot}772\chi^{0{\cdot}02054} \tag{29}$$

Maximum ripple height is predicted by the Mogridge *et al.* (1994) model as

$$\log_{10}(\eta/D) = 8{\cdot}542 - 10{\cdot}822\chi^{0{\cdot}03967} \tag{30}$$

which was derived from laboratory data.

Model of Wiberg & Harris (1994)

The model of Wiberg & Harris (1994) predicts ripple wavelength for three different relationships depending on whether the ripples are orbital, suborbital or anorbital. This is based on the value of the ratio d_o/η_{ano} where η_{ano} is anorbital ripple height. Therefore, it is necessary first to predict anorbital ripple height before determining what type of ripples will be present. Anorbital ripple steepness is predicted by iteration using the following relationship

$$\frac{\eta_{ano}}{\lambda} = \exp\left[-0{\cdot}095\left[\ln\frac{d_o}{\eta_{ano}}\right]^2 + 0{\cdot}442\,\ln\frac{d_o}{\eta_{ano}} - 2{\cdot}28\right] \quad (31)$$

If $d_o/\eta_{ano} < 20$, then the ripples are orbital ripples and

$$\lambda = 0{\cdot}62 d_o \quad (32)$$

$$\eta/\lambda = 0{\cdot}17 \quad (33)$$

When $20 < d_o/\eta_{ano} < 100$, suborbital ripples occur and

$$\lambda = \exp\left[\left[\frac{\ln(d_o/\eta_{ano}) - \ln 100}{\ln 20 - \ln 100}\right](\ln\lambda_{orb} - \ln\lambda_{ano}) + \ln\lambda_{ano}\right] \quad (34)$$

which is a weighted geometric average between values of orbital and anorbital ripple wavelength. Suborbital ripple height is calculated as the product of suborbital ripple wavelength and the ripple steepness from Eq 31. At values of $d_o/\eta_{ano} > 100$, the ripples are anorbital ripples and are defined as

$$\lambda = 535D \quad (35)$$

RESULTS

Sediment size distribution

Descriptive statistics for sediment size for each beach are shown by cross-shore location in Figs 2–5. The first sample was generally taken from the step at the foot of the beach face, which was defined as zero distance, and then from each subsequent ripple trough and crest. Samples were taken from two parallel profiles several metres apart at Garden Island, Jurien Jetty, Naval Park and Cockburn. Mean grain size (after the coarse material was sieved; Fig. 2) decreased with increasing distance from the shore at Bourlanger Point N., Garden Island, Naval Park and Rockingham. In addition to the decreasing trend found at those sites, all sites exhibited a 'saw-tooth' cross-shore variability that resulted from the differences in grain size at subsequent crests and troughs. This crest–trough differential was best seen at Jurien Jetty (Fig. 2F). Overall, among all the sediment samples, there was a significant difference (all tests at 0·05 significance level) in the mean grain sizes between crest and trough within the sand-sized fraction. Crests contained coarser sediment, and troughs contained finer sediment. Differences in mean size of sediment in crests and troughs for individual beaches are shown in Table 1. Three beaches in Cockburn Sound (Alexander St., Cockburn and Rockingham) did not show a significant difference in the mean grain size, although mean grain sizes at the crests were still greater than in the troughs.

The sand-sized fraction of all samples was well to moderately sorted (Fig. 3) with poorer sorting in the troughs and better sorting in the crests. This was best seen close to shore at Bourlanger Point N. and on both profiles at Naval Park (Fig. 3B and G). Sorting decreased in an offshore direction at Coolimba and Naval Park (Fig. 3D and G). Overall, more poorly sorted sediment was found in the troughs and better sorted material in the crests, except at Coolimba and Garden Island, where no significant difference was found (Table 1), although these two sites had the best sorted sand-sized fraction among the study sites.

The skewness of the sand-sized fraction followed trends similar to mean grain size (Fig. 4). Significantly, greater positive skewness (indicated by a tail of fines) was found in the crests at all sites except Rockingham and Cockburn (Table 1). Very few samples had negative skewness, but these occurred mainly at the offshore limits of the profiles, as skewness decreased steadily in an offshore direction at Bourlanger Point N., Naval Park and Rockingham (Fig. 4B, G and H).

Greater proportions of sediment coarser than 2 mm were found in the troughs than in the crests at all sites (Fig. 5). Only three sites, Bourlanger Point S., Coolimba and Jurien Jetty (Fig. 5C, D and F), showed no significant differences in the percentage of coarse material between crest and trough, and these sites had the least amount of coarse material (mean percentage coarse <0·25%). Hence, there was probably not enough coarser sediment to provide a significantly uneven distribution between crest and trough.

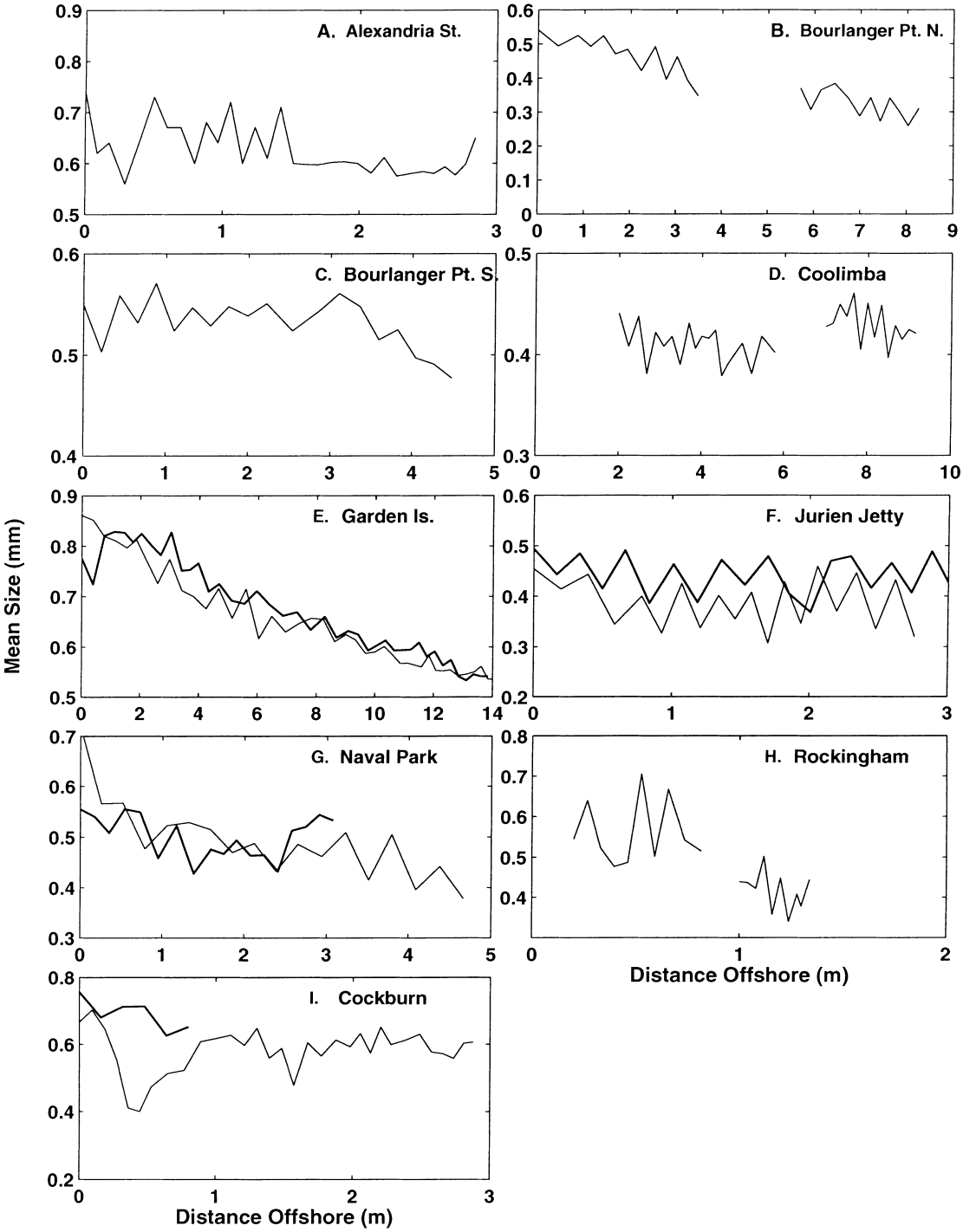

Fig. 2. Cross-shore distribution of mean grain sizes of the sand-sized sediment at each of the field sites. Bold lines plotted in (E), (F), (G) and (I) denote an additional cross-shore set of samples collected 2 m alongshore from the first line.

The descriptive statistics do not reveal all aspects of the sediment size distribution, and the actual size distributions show other differences between the crest and the trough. Sediment size distributions from four of the sites that best differentiate crest and trough sediments are shown in Fig. 6. Jurien Jetty sediment size distributions (Fig. 6A) clearly show the bimodal nature of the trough sediments compared with the unimodal crest sediments. Bourlanger Point N. and Coolimba (Fig. 6B and C) had very similar shapes for the distributions of crest and trough

Table 1. Summary of descriptive statistics for sediment samples from crests and troughs at each of the field sites.

		Sediment <2 mm							Paired samples *t*-test (*P*-values)			
Site	Location	Mean phi	mm	Sorting phi	mm	Skewness phi	mm	% Coarse (>2 mm)	C vs. T mean	C vs. T sorting	C vs. T skewness	C vs. T % coarse
Alexandra St.	Crests	0·79	0·58	0·59	0·18	2·29	−0·23	0·39	0·789	0·002	0·005	0
	Troughs	0·78	0·58	0·66	0·21	1·86	−0·14	3·51				
Bourlanger Pt. N.	Crests	1·42	0·37	0·54	0·14	0·87	0·76	0·46	0·005	0·002	0	0·005
	Troughs	1·61	0·33	0·63	0·17	0·16	1·20	1·08				
Bourlanger Pt. S.	Crests	0·94	0·52	0·50	0·13	3·30	−0·18	0·084	0·001	0·011	0·07	0·056
	Troughs	1·02	0·49	0·55	0·14	2·81	−0·29	0·2				
Coolimba	Crests	1·29	0·41	0·51	0·12	2·46	0·14	0·12	0	0·164	0	0·186
	Troughs	1·39	0·38	0·53	0·13	1·71	0·82	0·23				
Garden Is.	Crests	0·66	0·63	0·44	0·14	3·89	−0·03	1·92	0·001	0·854	0	0
	Troughs	0·7	0·62	0·44	0·15	3·57	0·04	4·08				
Jurien Jetty	Crests	1·28	0·41	0·65	0·16	1·28	−0·01	0·08	0	0·023	0	0·218
	Troughs	1·55	0·34	0·68	0·16	0·61	0·30	0·13				
Naval Park	Crests	1·14	0·45	0·71	0·21	0·88	0·14	0·54	0	0	0	0
	Troughs	1·33	0·40	0·82	0·24	0·47	0·36	2·07				
Rockingham	Crests	1·35	0·39	0·77	0·22	0·56	0·31	0·52	0·077	0	0·982	0·006
	Troughs	1·2	0·44	0·87	0·28	0·55	0·29	2·49				
Cockburn	Crests	0·94	0·52	0·67	0·21	1·88	0·14	0·7	0·223	0·037	0·237	0
	Troughs	0·9	0·54	0·73	0·23	1·72	0·08	3·52				

Test results of comparison between crest and trough size characteristics are also given.

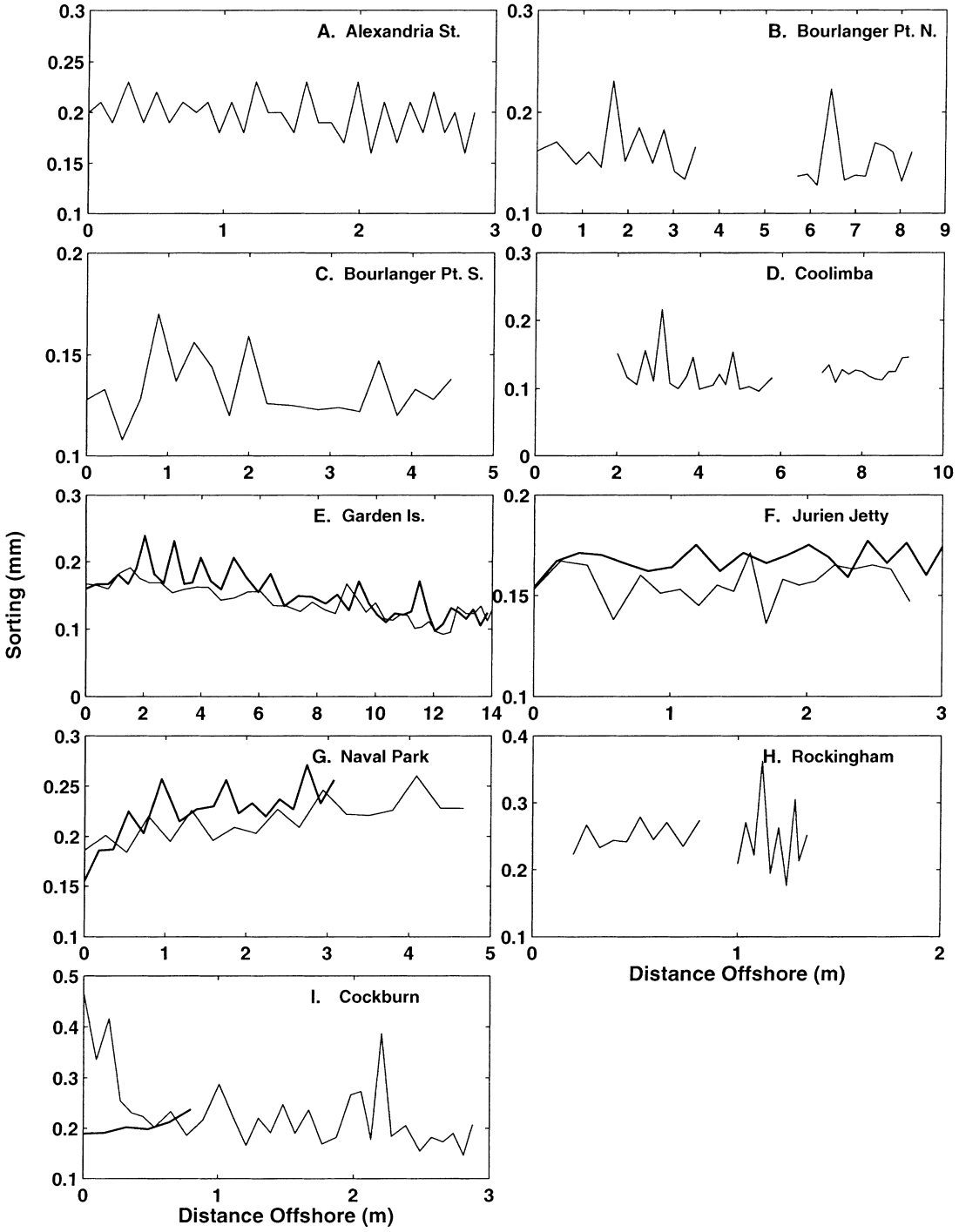

Fig. 3. Cross-shore distribution of the sorting of the sand-sized sediment at each of the field sites. Bold lines plotted in (E), (F), (G) and (I) denote an additional cross-shore set of samples collected 2 m alongshore from the first line.

sediments, except that the trough distributions were displaced towards the finer sizes. Naval Park (Fig. 6D) had similar distributions to those at Jurien Jetty with bimodal distributions in the troughs and generally unimodal distributions in the crests.

Predictive models of ripple geometry

Spatial predictions

The hydrodynamic input used in the predictive models of ripple geometry is summarized in Table 2. The ripple wavelength and height in

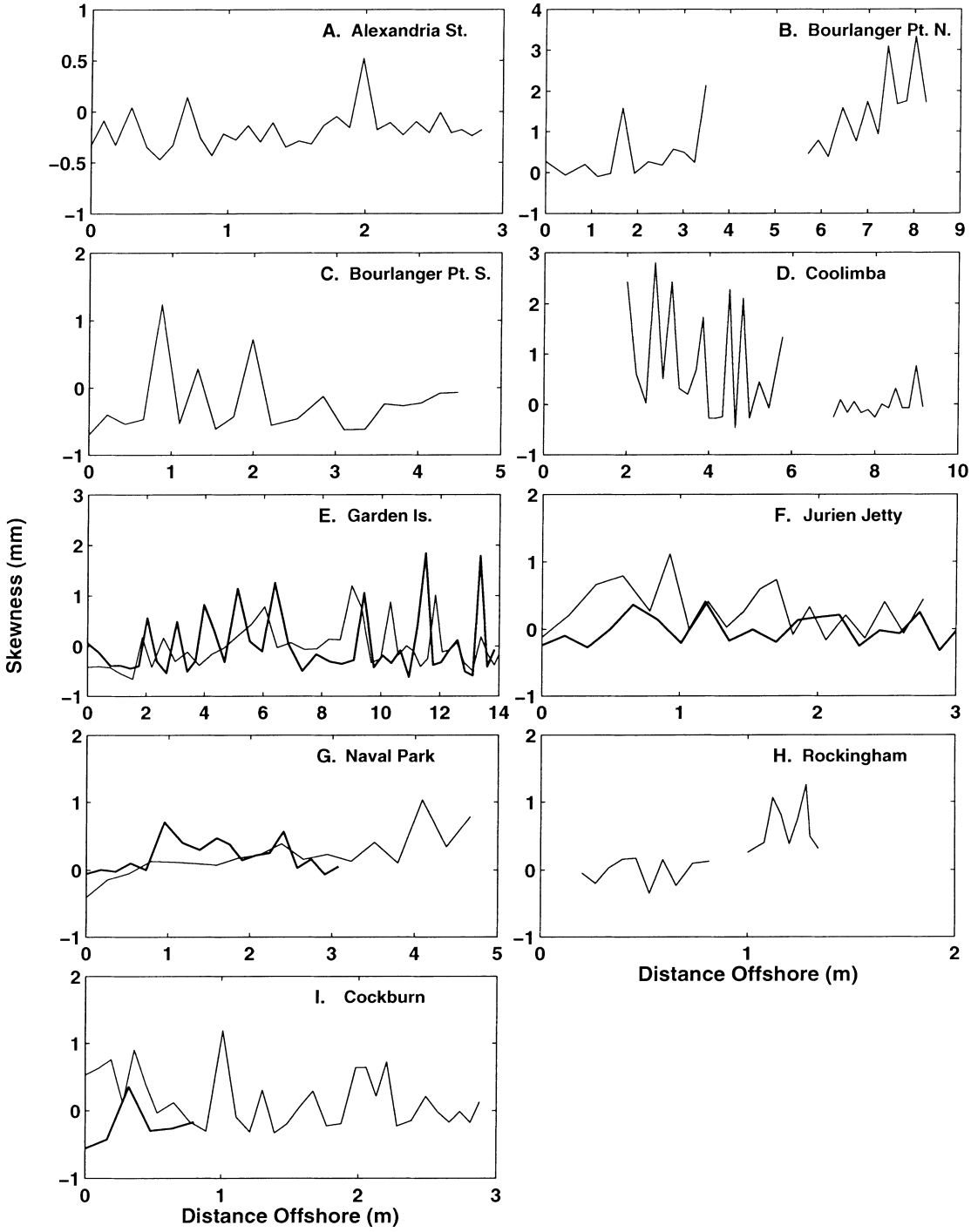

Fig. 4. Cross-shore distribution of the skewness of the sand-sized sediment at each of the field sites. Bold lines plotted in (E), (F), (G) and (I) denote an additional cross-shore set of samples collected 2 m alongshore from the first line.

Table 2 were averaged for four to six ripples adjacent to each pressure sensor location. Ripple wavelengths and heights predicted using both crest and trough mean sediment sizes were compared with the observed ripple wavelength at each pressure sensor location (Figs 7 and 8). The performance of the wavelength prediction models was assessed with the discrepancy ratio, R_d (Tables 3 and 4), where

$$R_d = \lambda_{predicted}/\lambda_{observed} \quad (36)$$

An R_d value of 1 is perfect agreement whereas $R_d > 1$ shows overprediction and $R_d < 1$ shows

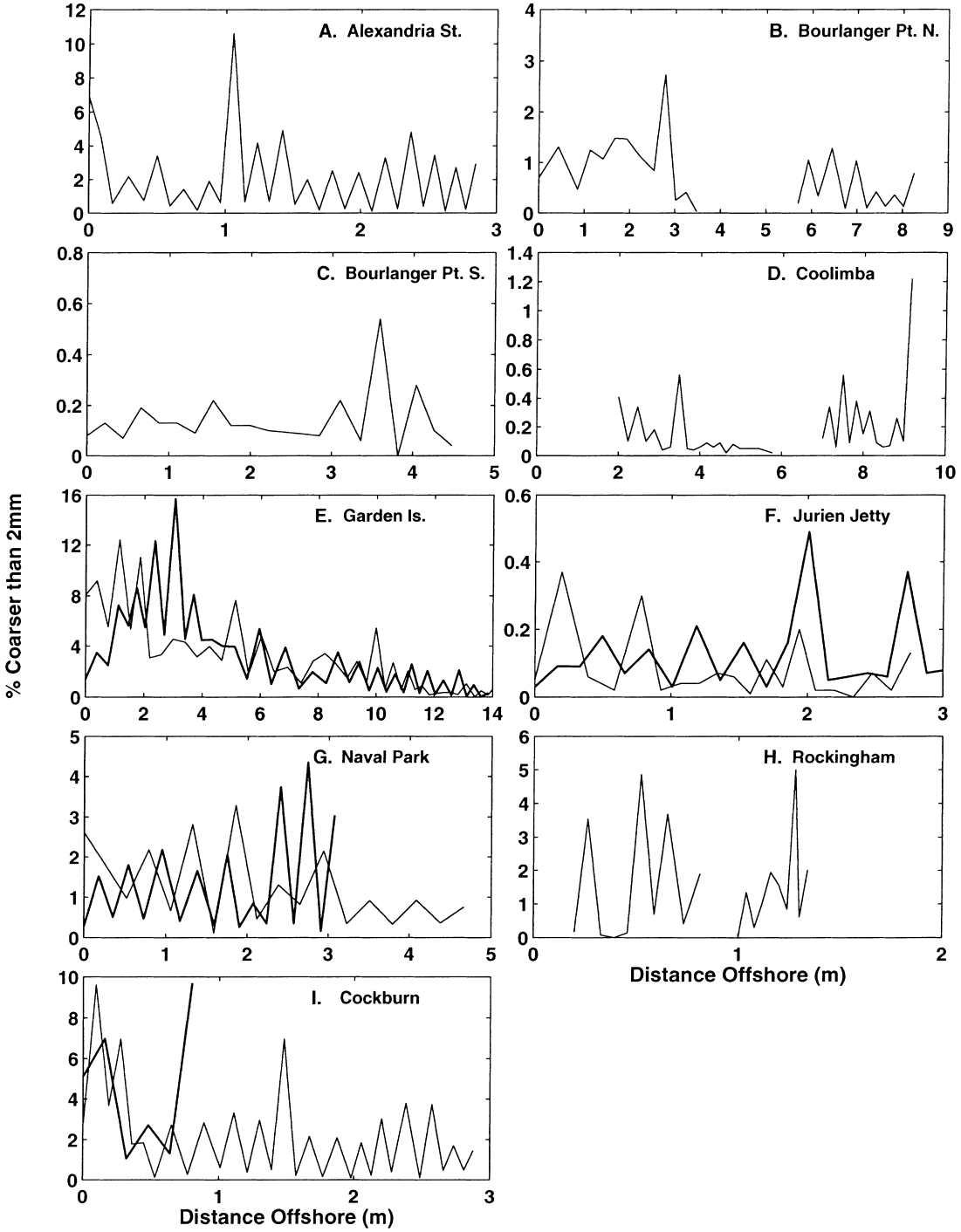

Fig. 5. Cross-shore distribution of the proportion of sediment coarser than sand size (>2 mm) at each of the field sites. Bold lines plotted in (E), (F), (G) and (I) denote an additional cross-shore set of samples collected 2 m alongshore from the first line.

underprediction. The discrepancy ratios are summarized by the mean geometric deviation (MGD) (Chandler & Kostaschuk, 1994; Villard & Kostaschuk, 1998)

$$\mathrm{MGD} = (R_{\mathrm{d}1} \times R_{\mathrm{d}2} \times R_{\mathrm{d}3} \ldots R_{\mathrm{d}n})^{1/n} \qquad (37)$$

where discrepancy ratios of less than 1 are replaced by their reciprocal. MGD values of 1 denote perfect agreement, and model performance decreases with increasing MGD values (Tables 3 and 4).

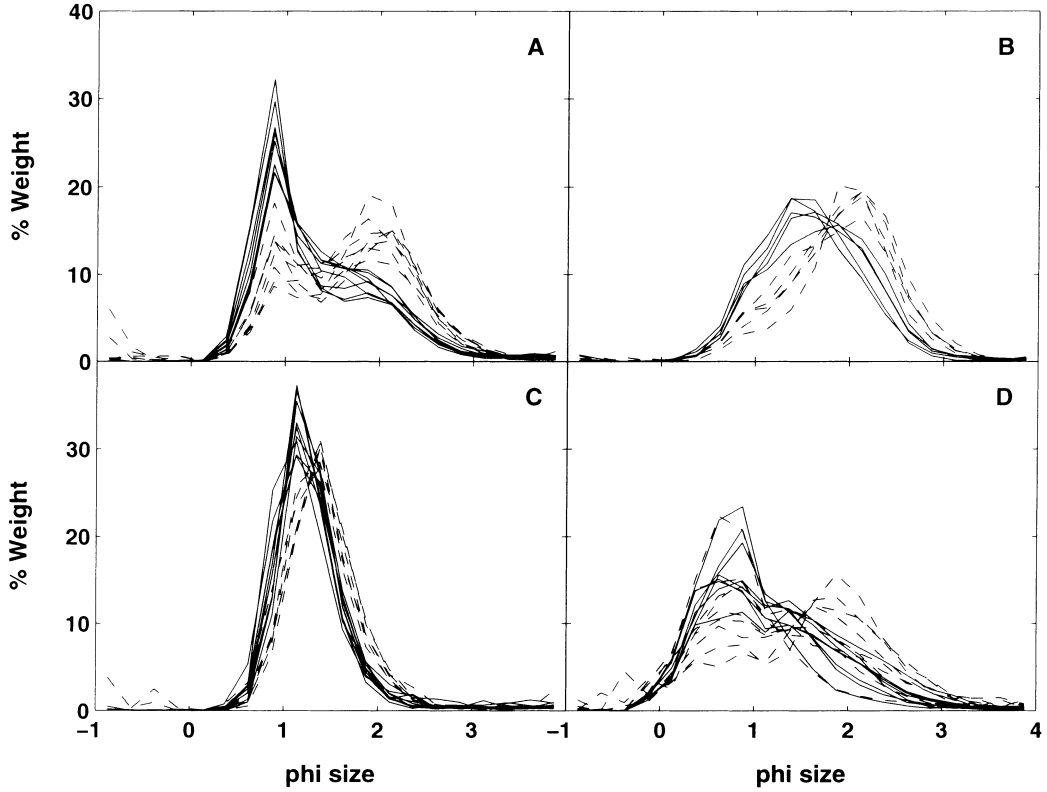

Fig. 6. Grain-size distributions for ripple crests (solid lines) and ripple troughs (dashed lines) for (A) Jurien Jetty, (B) Bourlanger Point N., (C) Coolimba and (D) Naval Park.

There was little difference in the ripple geometries predicted by the crest and trough mean sediment sizes for all the models except the Wikramanayake (1993) model, in which resulting wavelength prediction, using crest mean sediment sizes, was up to 44% higher than predictions made using the adjacent trough mean sediment size. Differences in ripple height predictions of up to 70% were found between predictions made with crest mean sediment sizes and trough mean sediment sizes. Some of the larger disparities were a result of values of the Wikramanayake (1993) non-dimensional parameter, Z, being very close to their threshold of 0·012 depending on which portion of the ripple the sediment sizes were taken from. Overall, among the other models, there was no significant difference in the accuracy of predictions made by the input of crest or trough mean sediment sizes (Tables 3 and 4).

The Nielsen (1981) field model (MGD = 1·35) and the Wiberg & Harris (1994) model (MGD = 1·41) were the most accurate at predicting the ripple wavelengths here, but their predictions still varied from the observed ripple wavelengths by up to 70% (Fig. 7; Table 3). Standard deviations of the predicted ripple wavelength from the observed ripple wavelength for these two models were ≈0·2 m. The Nielsen (1981) laboratory model (MGD = 1·91) was the least accurate with predictions of up to 4·5 times greater than that observed, suggesting that the laboratory data were generally a poor representation of field conditions. The Mogridge *et al.* (1994), Wikramanayake (1993) and Grant & Madsen (1982) models, with MGD values of 1·48, 1·47 and 1·80, respectively, made similar predictions with standard deviations from the observed ripple wavelengths of ≈0·3 m.

Ripple heights were best predicted by the Wiberg & Harris (1994) model (MGD = 1·38) and the Nielsen (1981) laboratory model (MGD = 1·43). The Mogridge *et al.* (1994) model overpredicted all ripple heights with discrepancy ratios as high as 7·12.

Temporal predictions

Observations and predictions of ripple wavelength from the six models for the temporal changes at Garden Island are shown in Fig. 9 and Table 5. According to Clifton's (1976) definitions, conditions were orbital ($d_o/D < 1000$)

Table 2. Hydrodynamic conditions and ripple geometry at each site.

Site	H_{sig} (m)	T (s)	d_o (m)	h (m)	Wavelength (m)	Height (m)
Alexandra St.	0·10	2·18	0·17	0·30	0·17	0·03
Bourlanger Pt. N.	0·21	9·17	1·44	0·77	0·52	0·09
	0·19	8·22	1·03	0·99	0·47	0·09
Bourlanger Pt. S.	0·19	4·06	0·56	0·50	0·50	0·06
Coolimba	0·13	6·63	1·19	0·18	0·42	0·06
	0·14	8·90	0·92	0·52	0·33	0·05
Garden Is.	0·26	10·47	2·22	0·47	0·74	0·11
	0·18	8·82	0·99	0·68	0·84	0·14
	0·16	7·46	0·77	0·77	0·91	0·11
	0·18	7·20	0·73	0·94	0·76	0·11
	0·21	8·73	0·94	1·01	0·56	0·10
	0·24	10·01	1·21	1·08	0·48	0·07
	0·26	10·47	2·22	0·47	0·64	0·09
	0·18	8·82	0·99	0·68	0·64	0·10
	0·16	7·46	0·77	0·77	0·80	0·12
	0·18	7·20	0·73	0·94	0·90	0·13
	0·21	8·73	0·94	1·01	0·62	0·11
	0·24	10·01	1·21	1·08	0·52	0·07
Jurien Jetty	0·17	4·11	0·62	0·38	0·26	0·05
	0·17	4·11	0·62	0·38	0·29	0·05
Naval Park	0·09	11·30	1·14	0·22	0·56	0·05
	0·12	12·15	1·78	0·23	0·33	0·03
Rockingham	0·07	2·30	0·13	0·33	0·08	0·02
Cockburn	0·06	2·40	0·13	0·31	0·16	0·02
	0·08	2·72	0·16	0·36	0·32	0·03

during the sea breeze and suborbital ($1000 < d_o/D < 5000$) during the swell-dominated period. Ripple wavelength increased with increasing nearbed orbital diameter during the sea breezes, suggesting the presence of orbital ripples, and showed no relationship with nearbed orbital diameter during the swell-dominated period, suggesting the presence of suborbital ripples (Fig. 9).

In comparing the models of Nielsen (1981), the field model performed better during the swell-dominated period and the laboratory model performed better during the sea breeze (Fig. 9A). This was expected as the laboratory model was derived from wave tank or tube data with generally shorter wavelengths than those found in the field. These shorter period waves ($T = 5$ s) occurred during the sea breeze, with longer period waves ($T = 9$ s) being present during the swell-dominated period.

The Mogridge *et al.* (1994) model performed well during the first sea breeze but overpredicted wavelengths by up to 200% during the swell-dominated period (Fig. 9A). The Mogridge *et al.* (1994) model did not take into account the change in ripple regime between the sea breeze and the swell-dominated period. The wave period parameter (χ) was $>0{\cdot}15 \times 10^{-6}$ at all times denoting laboratory-like conditions.

The Wikramanayake (1993) model (Fig. 9B) performed similarly to the model of Mogridge *et al.* (1994). Predicted ripple wavelengths increased during the sea breeze as orbital ripples, but the model did not predict a change in ripple regime with the end of the sea breeze. Predicted wavelengths continued to increase with the increasing nearbed orbital diameter during the swell-dominated period.

The model of Grant & Madsen (1982) predicted the ripple regime as being below the break-off point (i.e. orbital) and nearly always underpredicted the ripple wavelength (Fig. 9B). The Wiberg & Harris (1994) model performance was very similar to that of Grant & Madsen (1982) as shown in Fig. 9 and Table 5 where MGD values were both 1·59.

The Nielsen (1981) field, Wikramanayake (1993), Grant & Madsen (1982), and Wiberg &

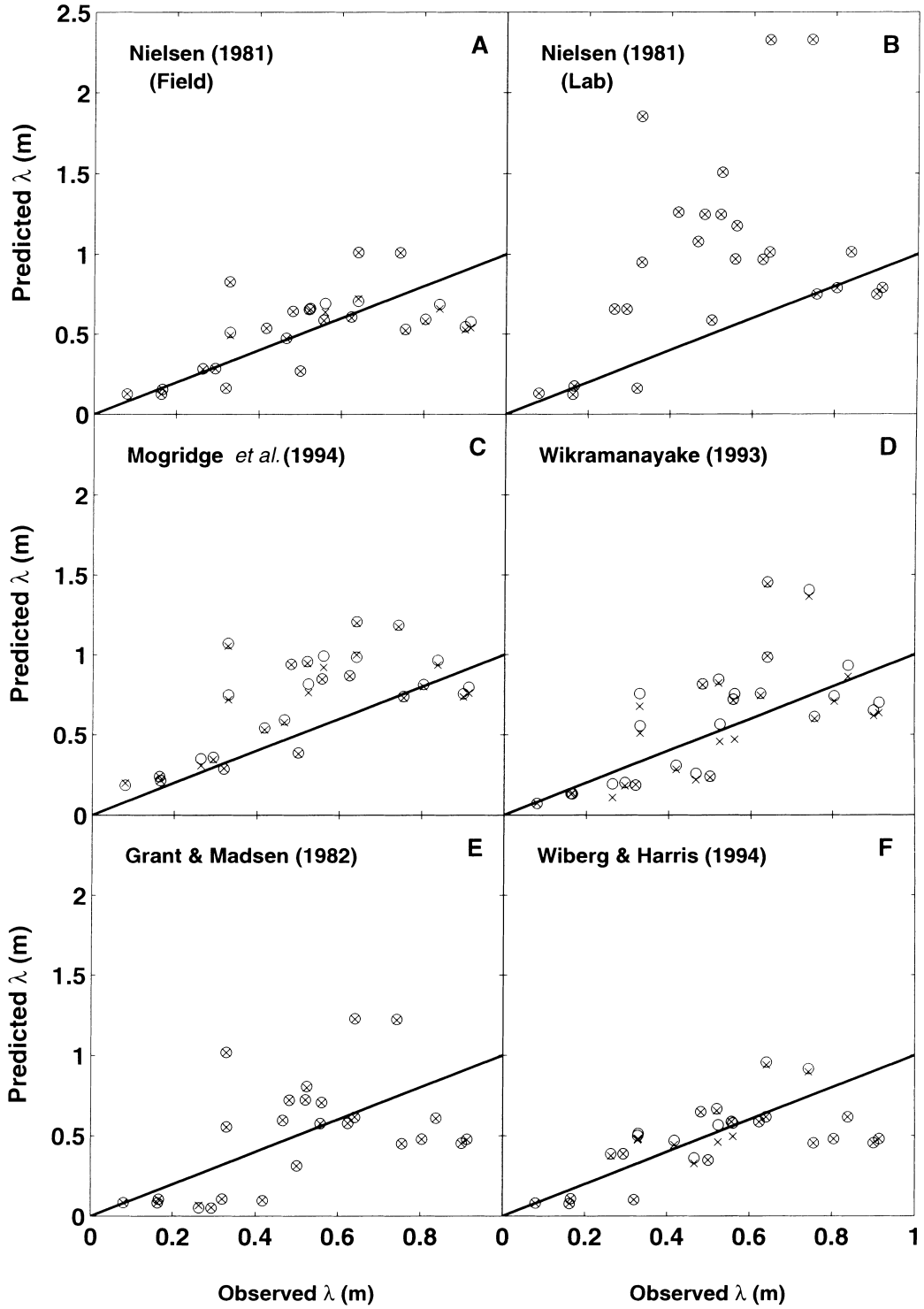

Fig. 7. Comparisons of predicted and observed ripple wavelengths for each of the models tested. Circles and crosses are the results using grain-size inputs from the crest and trough samples respectively.

Harris (1994) models all underpredict the ripple wavelength at the start of the second sea breeze (Fig. 9). Predicted ripple wavelengths were similar to those at the start of the first sea breeze as conditions were also similar, but the observed ripple wavelengths were different at the start of the second sea breeze. Observed ripple wavelengths fit the Clifton (1976) ripple regime classification where orbital ripples ($\lambda \propto d_o$) occur at $d_o/D < 1000$ and suborbital ripples ($\lambda \propto 1/d_o$)

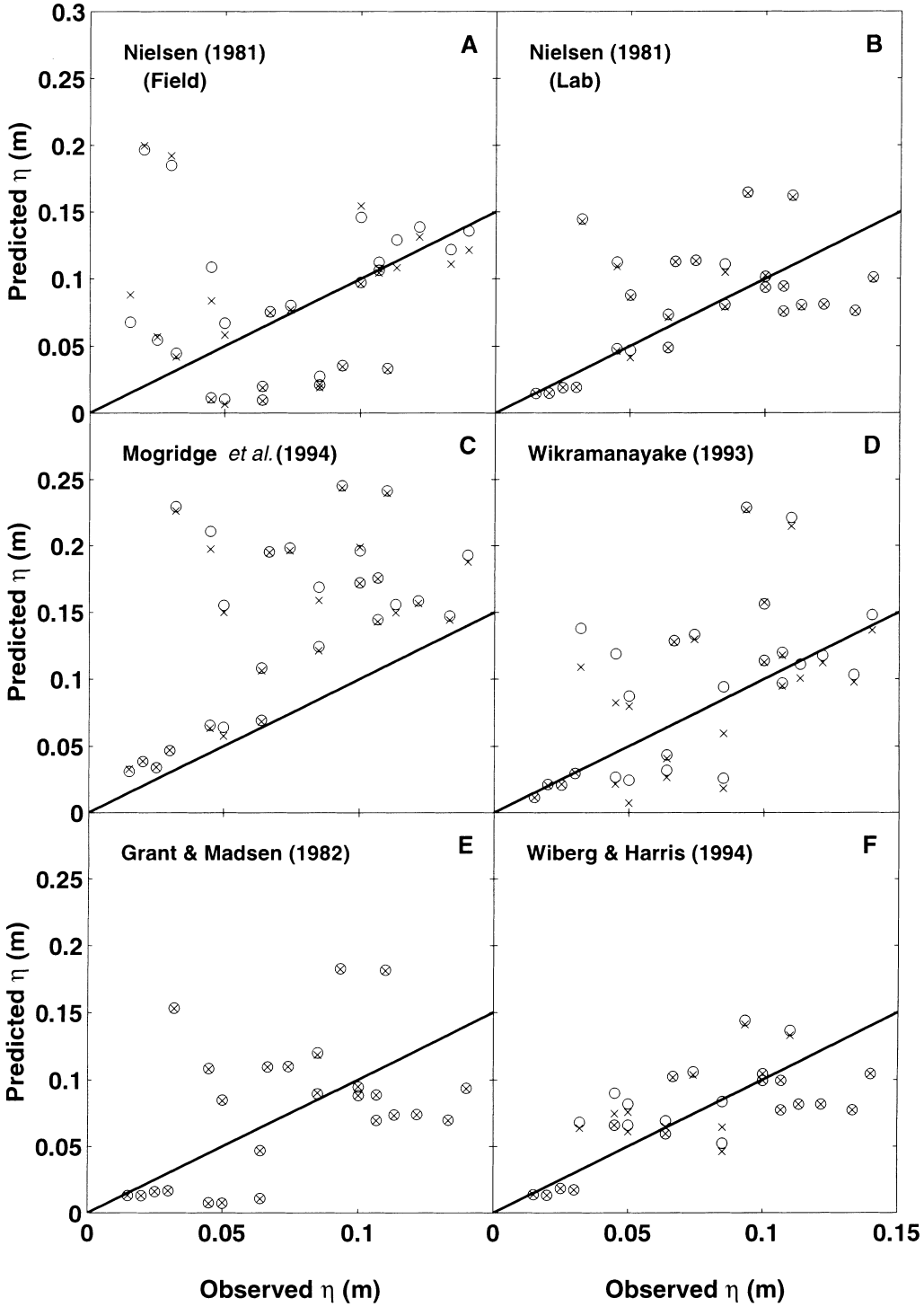

Fig. 8. Comparisons of predicted and observed ripple heights for each of the models tested. Circles and crosses are the results using grain-size inputs from the crest and trough samples respectively.

occur at $1000 < d_o/D < 5000$. Wavelength increased during the first sea breeze (orbital) and stayed relatively constant during the swell-dominated period (suborbital) before increasing again (orbital) during the second sea breeze. The ripple wavelength did not decrease to the same level as at the beginning of first sea breeze and, therefore, had a different 'starting wavelength' when the conditions became orbital again at the start of the second sea breeze. The history of the conditions at the bed was apparently important to the bed morphology at any point in time.

Table 3. Model performance statistics for ripple wavelength predictions.

Model	Crest sediments		Trough sediments		Average of crest and trough sediments	
	R_d	MGD	R_d	MGD	R_d	MGD
Nielsen (1981) Field	0·51–2·51	1·35	0·51–2·50	1·35	0·51–2·51	1·35
Nielsen (1981) Laboratory	0·51–5·64	1·91	0·51–5·64	1·91	0·51–5·64	1·91
Mogridge *et al.* (1994)	0·77–3·26	1·48	0·76–3·20	1·47	0·77–3·23	1·48
Wikramanayake (1993)	0·48–2·30	1·46	0·41–2·25	1·51	0·47–2·26	1·47
Grant & Madsen (1982)	0·17–3·09	1·81	0·18–3·09	1·79	0·18–3·09	1·80
Wiberg & Harris (1994)	0·32–1·55	1·41	0·32–1·47	1·41	0·32–1·51	1·41

Table 4. Model performance statistics for ripple height predictions.

Model	Crest sediments		Trough sediments		Average of crest and trough sediments	
	R_d	MGD	R_d	MGD	R_d	MGD
Nielsen (1981) Field	0·15–9·83	2·19	0·13–9·99	2·29	0·15–9·90	2·23
Nielsen (1981) Laboratory	0·57–4·51	1·43	0·57–4·46	1·43	0·57–1·08	1·43
Mogridge *et al.* (1994)	1·09–7·18	1·89	1·07–7·07	1·86	1·08–7·12	1·87
Wikramanayake (1993)	0·30–4·31	1·56	0·14–3·40	1·67	0·25–3·84	1·60
Grant & Madsen (1982)	0·15–4·79	1·86	0·15–4·78	1·87	0·14–4·78	1·87
Wiberg & Harris (1994)	0·58–2·13	1·38	0·54–1·98	1·37	0·57–2·05	1·38

DISCUSSION

Sediment size distribution

There are very few published measurements of sediment size distribution over individual ripples in the field. The results of this study, in which overall ripple crests were coarser, better sorted and more positively skewed than the troughs, were similar to the observations made by Inman (1957) in deeper water further offshore. Inman (1957) found coarser, better sorted material in the crest and finer, more poorly sorted material in the trough with a few exceptions. These exceptions had large, poorly sorted material in the trough, which was similar to this study, where the majority of material larger than sand size was in the trough. Miller & Komar (1980) found no difference in the grain-size distributions between ripple crests and troughs. Their measurements were in either well-sorted fine or medium-grained sands. It is possible that the sand was too well sorted at their two sites for there to be a significant difference in sediment sizes in crest and troughs. Clifton *et al.* (1971) found fine sand in crests and coarser sand in troughs of lunate megaripples in the nearshore, which occur at a much higher energy regime than the parallel ripples observed here. The difference in grain-size distribution over lunate megaripples and parallel ripples suggests that they are formed and maintained by very different processes.

Laboratory studies have shown similar results to the field observations reported here. Foti (1993), Foti & Blondeaux (1995), Noda (1968), De Best & Bijker (1971) and Carter *et al.* (1973) all found that sediment sorting within ripples occurred under waves. Foti (1993) found that the peak in concentration of coarse material oscillates about the ripple crest over a wave cycle. The latter three studies were of standing wave conditions, where light particles were deposited at antinodes and heavier particles at the nodes.

The differences in grain-size distribution between the ripple crests and troughs show the selectivity of transport over ripples. At each site, similar grain sizes were present in both crests and troughs, but they occurred in different abundances (Fig. 6). Bed shear stresses vary over ripples, with highest shear stresses occurring at the ripple crest (Li *et al.*, 1997). This possibly resulted in winnowing of the finer sediments from the crests making them coarser and better sorted with a positive skewness. This was best illustrated by the size distributions at Jurien Jetty (Fig. 6A), where a second mode of finer material was

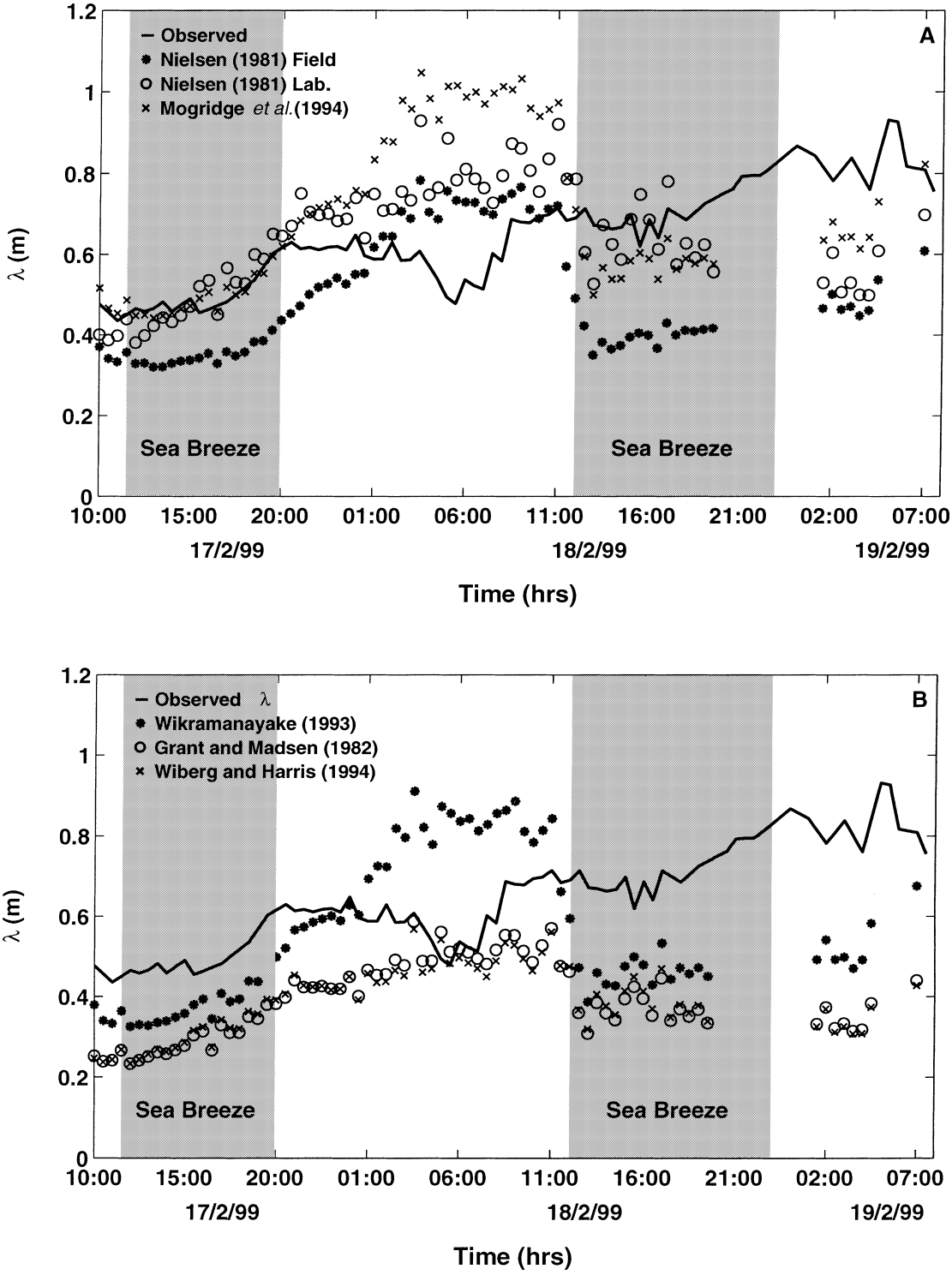

Fig. 9. Predicted and observed ripple wavelengths over time at Garden Island. Solid line is observed ripple wavelength. Shaded areas denote the sea breeze.

present in the trough but not at the crest. The majority of material coarser than sand was found in the trough, but this material was generally irregularly shaped shell hash or small pebbles that have very different hydraulic properties from the sand-sized material. It was possible that this material was too large to be maintained in the ripple crests by the leeside vortices and would probably slide or roll back into the trough if lifted onto the crest.

Table 5. Model performance statistics for temporal ripple wavelength predictions at the Garden Is. site.

Model	R_d	MGD
Nielsen (1981) Field	0·52–1·53	1·40
Nielsen (1981) Laboratory	0·63–1·79	1·20
Mogridge *et al.* (1994)	0·75–2·12	1·25
Wikramanayake (1993)	0·58–1·79	1·34
Grant & Madsen (1982)	0·39–1·13	1·59
Wiberg & Harris (1994)	0·38–1·10	1·59

Predictive models of ripple geometry

Spatial predictions

The Wikramanayake (1993) model was the most sensitive to grain-size input as the calculation of their non-dimensional parameter, Z, includes the cube of grain size. Inman (1957) stated that the grain sizes in the ripple crests are the most important for determining ripple wavelength, but neither crest nor trough sediment size was found to give more accurate model outputs in this study. Owing to the low energy at the study sites, most models predicted that the conditions were orbital or below the break-off point. Predictions of ripple wavelength under these conditions were not as dependent on grain size as under higher energy conditions where anorbital ripples are present. For example, the models of Mogridge *et al.* (1994) and Wiberg & Harris (1994) predict wavelength to be entirely dependent on grain size when anorbital ripples are present. Under the low-energy conditions here, observed wavelength was slightly better correlated with crest grain size ($r = 0{\cdot}58$) than trough grain size ($r = 0{\cdot}47$), suggesting that crest sediments do seem to be more important for determining ripple wavelength.

Accurate prediction of ripple dimensions is necessary to provide a measure of the degree of bed roughness or frictional drag, which is crucial for calculations of sediment transport by waves and currents (Grant & Madsen, 1982; Li, 1994; Li *et al.*, 1996; Mathisen & Madsen, 1996). The field model of Nielsen (1981) and the model of Wiberg & Harris (1994) were the best out of the models tested for predicting ripple wavelength. The model of Wiberg & Harris (1994) was also the best model for predicting ripple height. However, errors of prediction for these models were still large, with discrepancy ratios ranging from 0·32 to 2·51. Refinement of these models or the development of new models is needed for accurate predictions of bed roughness on low-energy microtidal beaches.

The laboratory model of Nielsen (1981) was the poorest model for predicting ripple wavelengths, although Vincent *et al.* (1999) found it was the only model that was able to predict the megaripples in their study. The laboratory model of Nielsen (1981) overpredicted ripple wavelength with discrepancy ratios as high as 5·64 (Fig. 7B and Table 3). It was possible that megaripples of the size predicted by the Nielsen model were not present here because of the occurrence of a wide wave spectrum. Additionally, Nielsen's (1981) laboratory model was not designed to work under the irregular wave conditions present in the field. The regular occurrence of afternoon sea breezes at all the study sites may have prevented long-term ripple growth under a narrow wave spectrum, which may have been required to develop megaripples.

Osborne & Vincent (1993) found that predictive models for ripple geometry performed poorly in macrotidal environments and attributed this partially to the rapidly changing hydrodynamic conditions resulting from tidal water level fluctuations. Although these models could be expected to perform better in the microtidal low-energy nearshore environment of Western Australia, where conditions are uniform for greater lengths of time, this was not found. There are several possible reasons for this. First, the models were based on laboratory data where ripples were generally produced under monochromatic wave conditions. In the field, where irregular waves were present, there may be no dominant orbital excursion to which the ripples can respond (Nielsen, 1981). The models would then overpredict ripple geometry as they are based on some representative parameter such as mean or maximum nearbed orbital excursion, rather than taking into account the whole spectrum of values present. Secondly, Foti (1993) found that sand of mixed sizes produced longer ripple wavelengths than those for uniform sand. As most laboratory studies used uniform sands for their experiments, the models generated from laboratory data could underpredict wavelength in the field where non-uniform sands are present. Thirdly, input and output parameters could be calculated slightly differently among the models. For example, the model of Mogridge *et al.* (1994) generally overpredicted ripple dimensions as it predicts maximum rather than mean ripple dimensions.

Temporal predictions

The inaccuracy of the model predictions over time (Fig. 9) suggests two further reasons why the models did not perform well in field conditions. First, the models failed to predict changes in the ripple regime that occurred at the beginning and end of the sea breezes. The small changes to the incident wave field resulting from the sea breeze caused a change from orbital to suborbital conditions that was not identified in the models. As the models were formulated using mostly laboratory data, they are not designed for the long-period, low-energy waves at these sites. The wide spectrum of waves in the field also makes it difficult to use simple parameters such as a single representative nearbed orbital diameter and/or wave period to characterize the hydrodynamic conditions (Marsh *et al.*, 1999). Dick *et al.* (1994) showed another example of the difficulty in identifying ripple regimes in the field where the model of Wiberg & Harris (1994) predicted anorbital ripples when an upper plane bed was present. Secondly, there is the possibility that different equilibrium forms could occur under the same conditions. The measurement of ripple wavelength over time showed that the wave and ripple history was very important. The ripple wavelength grew during both the first and the second sea breeze, but there was a different 'starting' wavelength at the beginning of the second sea breeze. The ripples at the beginning of each sea breeze were not 'relict' forms because the ripples always appeared to be active by constantly adjusting to the changing conditions. Therefore, there must be different equilibrium forms under the same conditions, or the conditions only appear the same when mean wave parameters are considered.

CONCLUSIONS

The following conclusions are made from this study concerning grain-size distribution over ripples and the prediction of ripple geometries on low-energy beaches with long-period, low-amplitude waves.

1 Overall, the ripple crests were significantly coarser, better sorted and more positively skewed than the troughs when considering only the sand-sized sediment. The troughs contained a greater proportion of sediment larger than sand size (>2 mm) than the crests.

2 The Wikramanayake (1993) model was the most sensitive to grain-size variations but, overall, there was no significant difference in ripple geometry predicted using crest or trough sediment sizes.

3 The field model of Nielsen (1981) and the model of Wiberg & Harris (1994) were the best models for predicting ripple wavelength of parallel ripples. The Wiberg & Harris (1994) model was also the most accurate model for predicting ripple height. It is suggested that these models should be used for the prediction of ripple geometry in low-energy microtidal nearshore environments.

4 The responses of ripple wavelength to changing hydrodynamic conditions depend on the history of the bed morphology.

ACKNOWLEDGEMENTS

Many thanks to my field helpers, Andreas Bollhoefer, Sarah Grimes, Jas Lapinski and Amanda Maxwell. Critical comments on the paper by Ian Eliot and David Johnson were greatly appreciated. Additional comments and suggestions by Jim Best, Paul Villard and an anonymous reviewer were also appreciated. Thanks also to Boyd Wykes for organizing access to the Garden Island field site. This work was completed while I was sponsored by a Natural Sciences and Engineering Research Council of Canada Post Graduate Award.

NOMENCLATURE

a_s	nearbed orbital amplitude
d_o	nearbed orbital diameter
d_{50}	median grain size
D	mean grain diameter
D_*	dimensionless sediment parameter (van Rijn, 1989)
f_w	wave friction factor
g	acceleration due to gravity
h	mean water depth
H	significant wave height
k	wave number
k_s	bed roughness height
L	wave length
MGD	mean geometric deviation
R_d	discrepancy ratio
s	specific density of sand
S_*	dimensionless sediment parameter
u_m	mean nearbed orbital velocity

u_{*wm} maximum skin friction wave shear velocity
χ wave period parameter
Z non-dimensional parameter
γ_s specific weight of sediment
θ maximum skin friction wave Shields parameter
θ_B break-off Shields parameter
θ_{cr} sediment threshold Shields parameter
η ripple height
η_{ano} anorbital ripple height
λ ripple wavelength
λ_{orb} orbital ripple wavelength
λ_{ano} anorbital ripple wavelength
ν kinematic viscosity
ψ mobility number
ω wave radian frequency

REFERENCES

Black, K.P. and **Oldman, J.W.** (1999) Wave mechanisms responsible for grain sorting and non-uniform ripple distribution across two moderate-energy, sandy continental shelves. *Mar. Geol.*, **162,** 121–132.

Carstens, M.R., Neilson, R.M. and **Altinbilek, H.D.** (1969) Bedforms generated in the laboratory under oscillatory flow: analytical and experimental study. *US Army Corps Eng., Coastal Eng. Res. Cent., Techn Mem.*, **28,** 39pp.

Carter, T.G., Liu, P.L.F. and **Mei, C.C.** (1973) Mass transport by waves and offshore sand bedforms. *J. Waterw. Port Coast. Eng.*, **99,** 65–184.

Chandler, T.J. and **Kostaschuk, R.A.** (1994) Test of selected bed-material load transport models. *Can. J. Civ. Eng.*, **21,** 770–777.

Clifton, H.E. (1976) Wave-formed sedimentary structures – a conceptual model. In: *Beach and Nearshore Sedimentation* (Eds R.A. Davis, Jr and R.L. Ethington), *Spec. Publ. SEPM*, **24,** 126–148.

Clifton, H.E., Hunter, R.E. and **Phillips, R.L.** (1971) Depositional structures and processes in the non-barred high-energy nearshore. *J. Sed. Petrol.*, **41,** 651–670.

De Best, A. and **Bijker, E.W.** (1971) Scouring of a sand bed in front of a vertical breakwater. Communications on Hydraulics, Report 71-1. Department of Civil Engineering, Delft University of Technology, Delft, The Netherlands.

Department of Defence (2000) *Australian National Tide Tables 1998.* Australian Hydrographic Publication 18. Department of Defence, Adelaide, Australia, 282 pp.

Dick, J.E., Erdman, M.R. and **Hanes, D.M.** (1994) Suspended sand concentration events due to shoaled waves over a flat be. *Mar. Geol.*, **119,** 67–73.

Dingler, J.R. (1974) Wave formed Ripple in Nearshore Sands. PhD Thesis, University of California, San Diego, 136 pp.

Foti, E. (1993) Grain sorting over ripples: preliminary results of an experimental investigation. In: *Sediment Transport Mechanisms in Coastal Environments and Rivers – Euromech 310* (Eds M. Belorgey, R.D. Rajzona and J.F.A. Sleath), pp. 311–321. World Scientific, London.

Foti, E. and **Blondeaux, P.** (1995) Sea ripple formation: the heterogeneous sediment case. *Coast. Eng.*, **25,** 237–253.

Grant, W.D. and **Madsen, O.S.** (1982) Movable bed roughness in unsteady oscillatory flow. *J. Geophys. Res.*, **87,** 469–481.

Greenwood, B. and **Davidson-Arnott, R.G.D.** (1972) Textural variation in the subenvironments of the shallow-water wave zone, Kouchibouguas Bay, New Brunswick. *Can. J. Earth Sci.*, **9,** 679–688.

Hallermeier, R.J. (1981) Terminal settling velocity of commonly occurring sand grains. *Sedimentology*, **28,** 859–865.

Hegge, J.H. (1994) *Low-energy Sandy Beaches of Southwestern Australia: Two-dimensional Morphology, Sediments and Dynamics*. Unpubl. PhD Thesis, University of Western Australia, 419 pp.

Inman, D.L. (1953) Areal and seasonal variations in beach and nearshore sediments at La Jolla, California. *US Army Corps of Engineers Beach Erosion Board, Technical Memorandum* **39**.

Inman, D.L. (1957) Wave-generated ripples in nearshore sands. *US Army Corps of Engineers, Beach Erosion Board, Technical Memorandum*, **100,** 67 pp.

Kench, P.S. (1998) Physical controls on development of lagoon sand deposits and lagoon infilling in an Indian Ocean atoll. *J. Coast. Res.*, **14,** 1014–1024.

Kench, P.S. and **McLean, R.F.** (1997) A comparison of settling and sieve techniques for the analysis of bioclastic sediments. *Sed. Geol.*, **109,** 111–119.

Kennedy, J.F. and **Falcon, M.** (1965) *Wave-Generated Sediment Ripples*. Report 86. Massachusetts Institute of Technology, Cambridge, USA, 86 pp.

Li, M.Z. (1994) Direct skin friction measurements and stress partitioning over movable sand ripples. *J. Geophys. Res.*, **99,** 791–799.

Li, M.Z., Wright, L.D. and **Amos, C.L.** (1996) Predicting ripple roughness and sand resuspension under combined flows in a shoreface environment. *Mar. Geol.*, **130,** 139–161.

Li, M.Z., Amos, C.L. and **Heffler, D.E.** (1997) Boundary layer dynamics and sediment transport under storm and non-storm conditions on the Scotian Shelf. *Mar. Geol.*, **141,** 157–181.

McLaren, P. and **Bowles, D.** (1985) The effects of sediment transport on grain-size distributions. *J. Sed. Petrol.*, **55,** 457–470.

Marsh, S.W., Vincent, C.E. and **Osborne, P.D.** (1999) Bedforms in a laboratory wave flume: an evaluation of predictive models for bedform wavelengths. *J. Coast. Res.*, **15,** 624–634.

Masselink, G. (1992) Longshore variation of grain size distribution along the coast of the Rhone Delta, southern France: a test of the 'McLaren model'. *J. Coast. Res.*, **8,** 286–291.

Mathisen, P.P. and **Madsen, O.S.** (1996) Waves and currents over a fixed rippled bed. *J. Geophys. Res.*, **101,** 16533–16550.

Medina, R., Losada, I.J. and **Vidal, C.** (1994) Temporal and spatial relationship between sediment grain size and beach profile. *Mar. Geol.*, **118,** 195–206.

Miller, M.C. and **Komar, P.D.** (1980) A field investigation of the relationship between oscillation ripple spacing and the near-bottom water orbital motions. *J. Sed. Petrol.*, **50,** 0183–0191.

Miller, R.L. and **Zeigler, J.M.** (1958) A model relating sediment pattern in the region of shoaling waves, breaker zone, and foreshore. *J. Geol.*, **66,** 417–441.

Mogridge, G.R. and **Kamphuis, J.W.** (1972) Experiment on bed-form generation by wave action. In: *Proceedings of the 13th Coastal Engineering Conference*, Vancouver, BC, ASCE, pp. 1123–1142.

Mogridge, G.R., Davies, M.H. and **Willis, D.H.** (1994) Geometry prediction for wave-generated bedforms. *Coast. Eng.*, **22,** 255–286.

Nielsen, P. (1979) Some basic concepts of wave sediment transport. Series Paper 20. Institute of Hydrodynamics and Hydraulic Engineering, Technical University of Denmark, Lyngby, 160 pp.

Nielsen, P. (1981) Dynamics and geometry of wave-generated ripples. *J. Geophys. Res.*, **86,** 6467–6472.

Noda, H. (1968) A study on mass transport in boundary layers in standing waves. In: *Proceedings of the 11th Coastal Engineering Conference*, London. UK, ACSE, pp. 227–235.

Osborne, P.D. and **Greenwood, B.** (1993) Sediment suspension under waves and currents: time scales and vertical structure. *Sedimentology*, **40,** 599–622.

Osborne, P.D. and **Vincent, C.E.** (1993) Dynamics of large and small scale bedforms on a macrotidal shoreface under shoaling and breaking waves. *Mar. Geol.*, **115,** 207–226.

van Rijn, L.C. (1989) *Handbook of Sediment Transport by Currents and Waves.* Delft Hydraulics, Delft.

Sanderson, P.G. and **Eliot, I.** (1999) Compartmentalisation of beachface sediments along the southwestern coast of Australia. *Mar. Geol.*, **162,** 145–164.

Swart, D.H. (1974) A Schematisation of onshore-offshore transport. In: *Proceedings of the 14th International Conference on Coastal Engineering*, Copenhagen, Denmark, ACSE pp. 1782–1798.

Villard, P. and **Kostaschuk, R.** (1998) The relationship between shear velocity and suspended sediment concentration over dunes: Fraser Estuary, Canada. *Mar. Geol.*, **148,** 71–81.

Vincent, C.E., Marsh, S., Webb, M. and **Osborne, P.D.** (1999) Spatial and temporal structures of suspension and transport over mega-ripples on the shore face. *J. Geophys. Res.*, **104,** 1215–11224.

Vincent, C.E. and **Osborne, P.D.** (1993) Bedform dimensions and migration rates under shoaling and breaking waves. *Cont. Shelf Res.*, **13,** 1267–1280.

Wiberg, P.L. and **Harris, C.K.** (1994) Ripple geometry in wave-dominated environments. *J. Geophys. Res.*, **99,** 775–789.

Wikramanayake, P.N. (1993) *Velocity Profiles and Suspended Sediment Transport in Wave-current Flows.* PhD Thesis, Massachusetts Institute of Technology, 285 pp.

Yalin, S. and **Russell, R.C.H.** (1962) Similarity in sediment transport due to waves. In: *Proceedings of the 8th Coastal Engineering Conference*, Mexico City, ASCE, pp. 151–167.

Manuscript received 18 January 2001;
revision accepted 10 December 2001.